https://doi.org/10.20965/jdr.2016.p0225

Paper:

Object-Based Method for Estimating Tsunami-Induced Damage Using TerraSAR-X Data

Hideomi Gokon*, **Shunichi Koshimura****, **and Masashi Matsuoka*****

*Institute of Industrial Science, The University of Tokyo
4-6-1-Be604, Komaba, Meguro-ku, Tokyo 153-8505, Japan
E-mail: gokon@iis.u-tokyo.ac.jp
**International Research Institute of Disaster Science, Tohoku University, Sendai, Japan
***Graduate School of Science and Technology, Tokyo Institute of Technology, Yokohama, Japan

[Received October 3, 2015; accepted January 6, 2016]

The object-based method we developed to estimate building damage uses high-resolution synthetic aperture radar (TerraSAR-X) data from the 2011 Tohoku earthquake and tsunami. The damage function we developed involves the relationship between changes in the sigma nought values of pre- and postevent TerraSAR-X data and the damage ratio of washed-away buildings. We confirmed that the function performed as expected by estimating the number of washed-away buildings in homogeneous areas, agreeing well with ground truth data verified by a Pearson fs correlation coefficient of 0.99. The same damage function applied at another test site yielded a Pearson's correlation coefficient of 0.98. These results are sufficient to ensure transferability. We then simplified and semiautomated these processes in an ArcGIS environment, estimating building damage in the city of Sendai within 26 minutes.

Keywords: Remote sensing, Building damage, Tsunami, SAR, Object-based method

1. Introduction

A Mw9.0 earthquake and tsunami occurred along the coast of the Tohoku region in northeast Japan on March 11, 2011. The tsunami had a maximum runup height of 40.1 m that caused major damage to buildings, forests, and the infrastructure, in addition to eroding the coastline [1]. As of August 10, 2014, Japan's National Police Agency had reported 18,499 dead or missing and 127,390 buildings and/or houses that had collapsed or been washed away in the tsunami [2]. Since 2011, we have studied the tsunami and its impact using such approaches as field surveys, numerical modeling and remote sensing [3, 4]. Individual approaches each have their advantages and disadvantages, so the optimal approach for a case should be selected based on the information required. Remote sensing technology is useful, for example, in assessing extensive damage, and synthetic aperture radar (SAR), which functions quasi regardless of weather and light conditions, enhances the rapid observation of affected areas [5].

Numerous methods for detecting building damage caused by natural disasters have been developed in recent decades [6–9] After the TerraSAR-X(DLR) and CosmoSkyMed, which have high-resolution active sensors, were launched in 2007, approaches have been based increasingly on a building unit scale that takes high-resolution SAR data into consideration [10–12]. In the 2011 Tohoku disaster, airborne high-spatial-resolution SAR has been used to assess building damage induced in tsunamis [13–15]. Another method that inspects detailed damage to building side walls based on the side looking system in SAR observation has been proposed for use following tsunami disasters [16].

Most among the several types of techniques for detecting building damage on a building unit scale have identified building damage based on changes in the sigma nought values of SAR data in the building silhouette. These models sometimes show errors, however, e.g., in cases where changes to the building silhouette change sigma nought values in the silhouette – one of the challenges when using a unit-scale-based method. To solve this silhouette problem, surrounding pixels should be used to identify building damage. That is, both changes in the silhouette and surrouding changes in the building itself should be considered in detecting building damage. We focused on such zonal changes, which are wider than the building-unit scale, with the objective of developing a new way for estimating buildings washed away by a tsunami.

2. Data Set and Study Area

The study area we selected was Sendai, a Miyagi Prefecture city that was one of the most devastated in the 2011 Tohoku earthquake and tsunami (**Fig. 1(A)**).We detected damage using pre- and postevent TerraSAR-X data. Preevent data was collected on October 20, 2010 (UTC) and postevent data on March 12, 2011 (UTC), by using strip map mode that originally provided 3 meters in spatial resolution. Data sets were offset (EEC) geometrically and resampled at a 1.25 m/pixel resolution (**Figs. 1(B)**, **(C)**). Results were validated using high-resolution preevent optical satellite images, Worldview-2 images taken on August 4, 2010 (UTC) (**Fig. 1(D)**), and

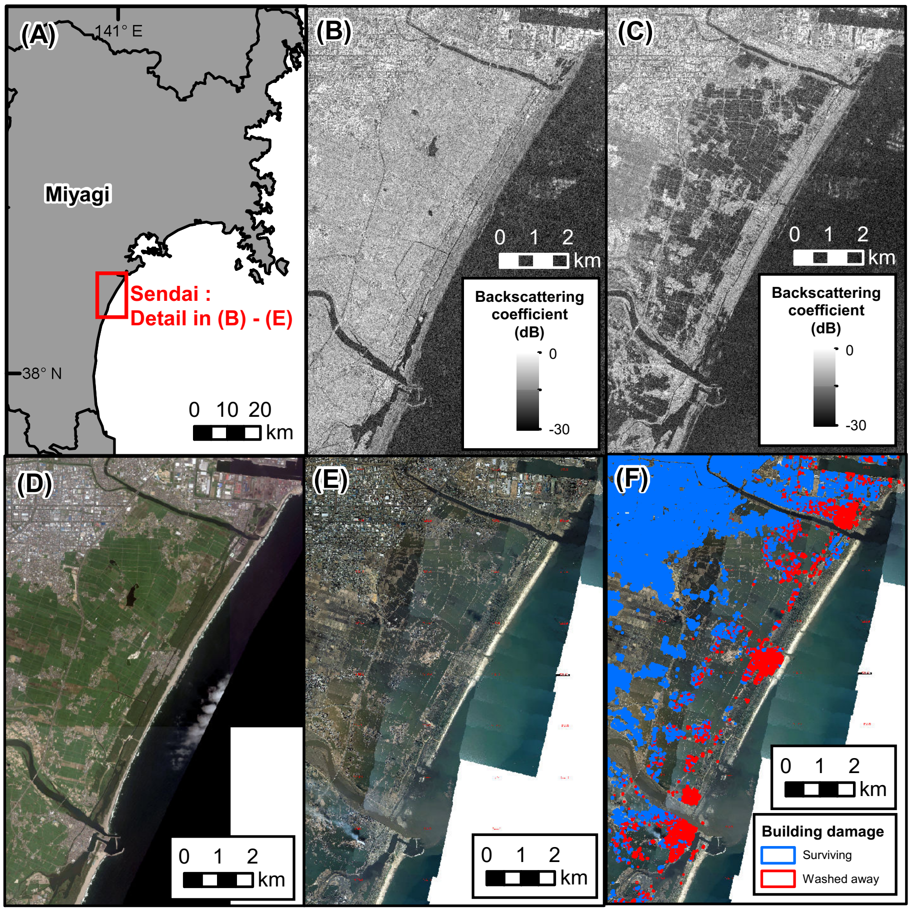

Fig. 1. (A) Study area, (B) Preevent TerraSAR-X data, (C) Postevent TerraSAR-X data, (D) Preevent Worldview-2 image, (E) Postevent Worldview-2 image, (F) Building damage data.

postevent aerial photographs taken on March 12, 2011 (JST), and provided by the Geospatial Information Authority of Japan (GSI) (**Fig. 1(E)**) [17]. Building damage map, i.e., building footprint data having "Survived" and "Washed a way" attributes was used (**Fig. 1(F)**) [18]. A building mask was extracted based on preevent building footprint data (Zmap-TOWNII) published by using Japan's Zenrin. TerraSAR-X data were preprocessed by using U.S. Exelis VIS ENVI ver. 5.0. TerraSAR-X data was mainly processed based on U.S. Trimble eCognition Developer ver. 8.64.0 and ArcGIS ver. 10.1.

3. Method

3.1. Pre-Processing

TerraSAR-X data preprocessing included calibration converting digital numbers to sigma nought (dB). Speckle noise was reduced by using a Lee filter with a 3×3 (3.75 m×3.75 m) window [19]. Last, pre- and postevent images were registered based on a normalized cross-correlation.

3.2. Change Detection

To detect changes caused by the tsunami, we calculated correlation coefficient images using pre- and postevent TerraSAR-X data (**Fig. 2**). Correlation coefficient (r) was defined as follows:

$$r = \frac{N\sum Ia_i Ib_i - \sum Ia_i \sum Ib_i}{\sqrt{(N\sum Ia_i^2 - (\sum Ia_i)^2)}\sqrt{(N\sum Ib_i^2 - (\sum Ib_i)^2)}} \quad (1)$$

where Ia_i and Ib_i are the sigma nought values of the ith number of pixels in the kernel. $\sum$ is the sum of ith pixel values, and N is the number of pixels in the kernel. Correlation coefficients ranged from -1 to $+1$. Areas with small changes showed higher values and those with large changes show lower values.

Correlation coefficient images were calculated based on five types of kernel sizes: 3.75 m × 3.75 m, 11.25 m × 11.25 m, 18.75 m × 18.75 m, 26.25 m × 26.25 m, 33.75 m × 33.75 m (**Figs. 2(A)** to **(E)**). Comparing correlation coefficient images to actual building damage distribution showed that surviving buildings were concentrated, showing a higher correlation coefficient. In areas where most buildings had been washed away by the tsunami, correlation coefficient images showed lower values. For correlation coefficient images calculated by a 3.75 m^2 kernel size, noise was confirmed throughout the image, making it difficult to identify boundaries of built-up areas. We inferred that these were caused by small changes in the earth's surface. As kernel size increased, these boundaries became clearer, however.

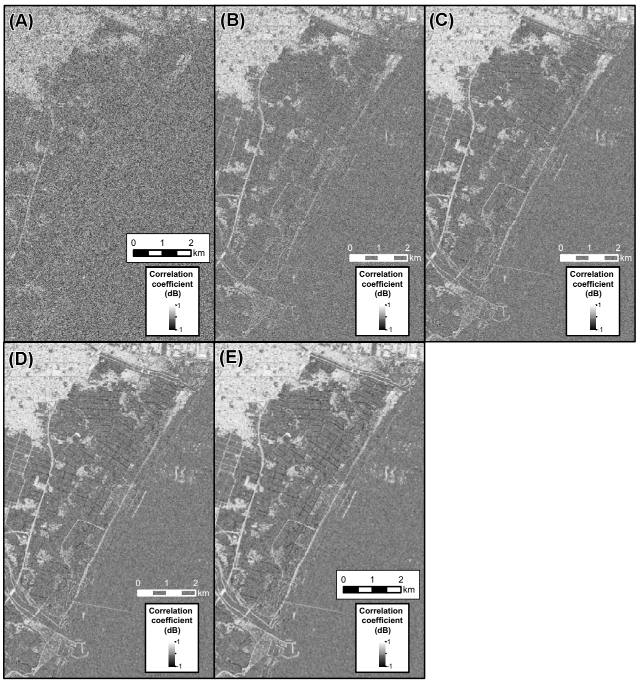

Fig. 2. Change detection by calculating correlation coefficient images. Kernel sizes for the calculations are; (A) 3.75 m× 3.75 m, (B) 11.25 m × 11.25 m, (C) 18.75 m×18.75 m, (D) 26.25 m × 26.25 m, (E) 33.75 m×33.75 m.

3.3. Investigation of the Relationship Between the Changes on the Ground and Correlation Coefficient Values

Changes on the ground caused changes in the backscattering coefficient, which in turn resulted in changes in correlation coefficient values. Before estimating building damage based on the correlation coeffient, we found it useful to investigate the relationship between ground changes in built-up areas and correlation coefficient values.

We studied cases of the following six ground change patterns in built-up areas:

- Case 1: Buildings were washed away and the site was covered by water (**Fig. 3(A)**).
- Case 2: Buildings were washed away and the foundation walls were exposed (**Fig. 3(B)**).
- Case 3: Buildings were washed away and the site was covered by soil (**Fig. 3(C)**).
- Case 4: Buildings were washed away and the site was covered by debris (**Fig. 3(D)**).
- Case 5: Buildings survived and debris accumulated around them (**Fig. 3(E)**).
- Case 6: Buildings survived and the site was covered by soil (**Fig. 3(F)**).

We calculated the mean correlation coefficient values inside red lines in **Fig. 3** as shown in **Fig. 4**. Note that mean correlation coefficient values decrease as ground changes become increasingly significant.

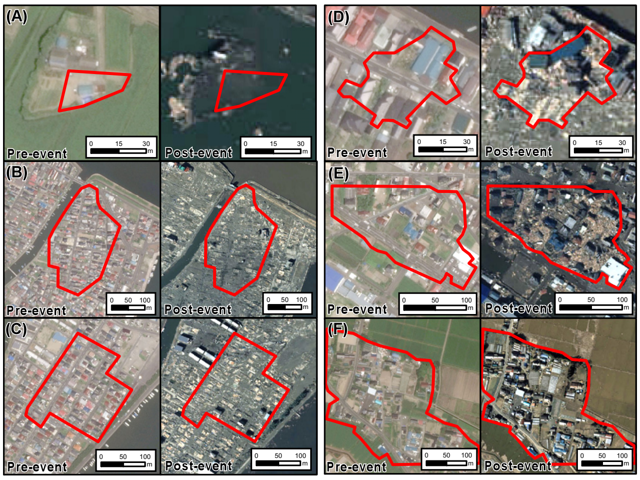

Fig. 3. Building damage in tsunami-affected areas (A) Case 1: Buildings were washed away and the site was covered by water; (B) Case 2: Buildings were washed away and foundation walls were exposed; (C) Case 3: Buildings were washed away and the site was covered by soil; (D) Case 4: Buildings were washed away and the site was covered by debris; (E) Case 5: Buildings survived and debris accumulated around them; (F) Case 6: Buildings survived and the site was covered by soil.

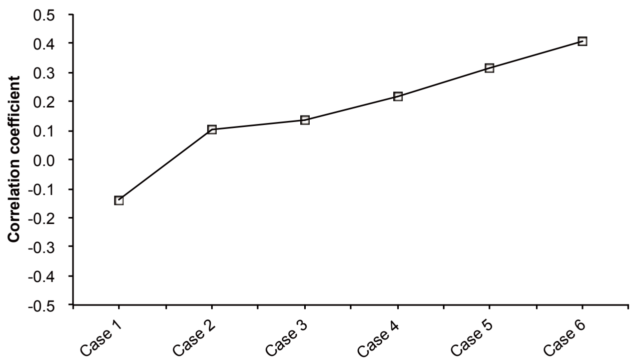

Fig. 4. Mean correlation coefficients based on damage pattern types.

3.4. Extraction of Built-Up Areas

To focus on changes related to building damage, we created a mask of built-up areas based on preevent building footprint data, i.e., Zmap-TOWNII. Specifically, we created outlines of built-up areas 10 meters from the building footprint and merged with each other using the ArcGIS buffer tool shown in **Figs. 5(A), (B)**.

3.5. Region Growing Method

To classify correlation coefficient images into areas with similar ground changes, we applied a region growthe method. Here we assumed that similar ground changes caused similar changes in backscattering coefficients, which led to similar patterns of correlation coefficient values.

Segmentation was based on the region growing method to classify correlation coefficient images based on the

Fig. 5. Example of region-growth-based segmentation. (A) Building footprint data, (B) Built-up area views, (C) An example of objects.

ground change features in the previous section. An example of segmentation is shown in (**Fig. 5(C)**). Correlation coefficient images within built-up areas were divided into objects based on homogeneity. We conducted segmentation processing based on the " multi-resolution segmentation" processing provided by the eCognition Developer. We determined segmentation parameters by trial and error in order to classify correlation coefficient images with the patterns defined in the previous section. We used the following final parameters to make objects: scale parameter: 200, shape: 0.1, color: 0.9, smoothness: 0.5 and compactness: 0.5.

3.6. Damage Function

To find the optimal kernel size for detecting building damage, we calculated and compared Pearson's correlation coefficients between mean correlation coefficient values for each object and the damage ratio as shown in **Fig. 6**. This resulted in our choosing a kernel size of 11.25 m $\times$ 11.25 m for estimating damage. We developed a damage function for estimating the damage ratios

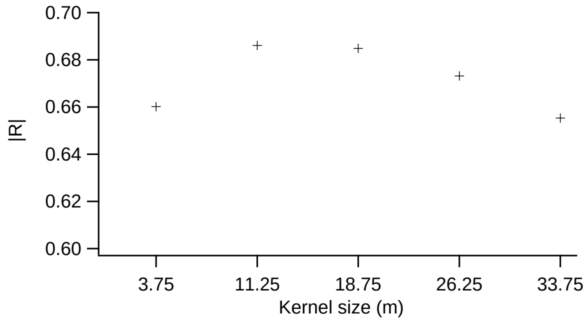

Fig. 6. Experimentally found optimal correlation coeffcient sizes. (|R|:Absolute value of correlation coefficient).

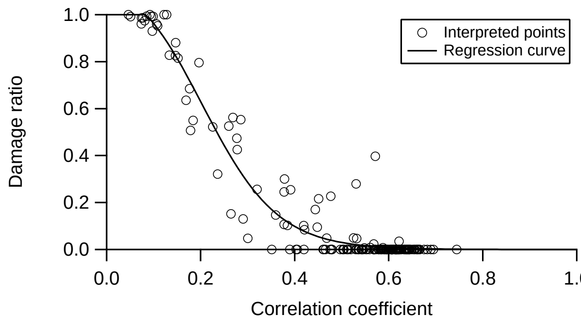

Fig. 7. Regression curve estimating the washed-away-building damage ratio.

of washed-away buildings on a zonal scale. Damage ratios were estimated by calculating the ratio of the number of washed away buildings over the total number of buildings within each object. We correoated mean values of correlation coefficients and damage ratios for development and conducted regression analysis. In this case, average correlation coefficient values were explanatory variables and damage ratios were predictors. We validated functions based on a building damage map having information on surviving and washed-away buildings as proposed by Gokon and Koshimura (2012) [20]. We conducted regression analysis using all of the objects with buildings numbering more than 30 in the study area, i.e., 182 objects. We used a sigmoid function for fitting as shown in **Fig. 7**. Derived function F is given as follows:

$$F = 1.20 - \frac{1.20}{\left(1+\exp\left(-\frac{R_m - 0.21}{0.080}\right)\right)} \quad . \; . \; . \quad (2)$$

where R_m is the mean value of a correlation coefficient in an object. In **Fig. 7**, a line shows a regression curve and points are damage ratios in individual objects. This function shows that for a low correlation coefficient, the damage ratio is high.

Some parts of objects showed higher damage ratios, even though the correlation coefficient was a high value exceeding 0.5. In investigating possible causes for this, we found that damage to objects that included large-scale buildings had been underestimated, i.e., even small buildings included in objects washed away by the tsunami showed correlation coefficient values higher by the large scale buildings surviving the tsunami.

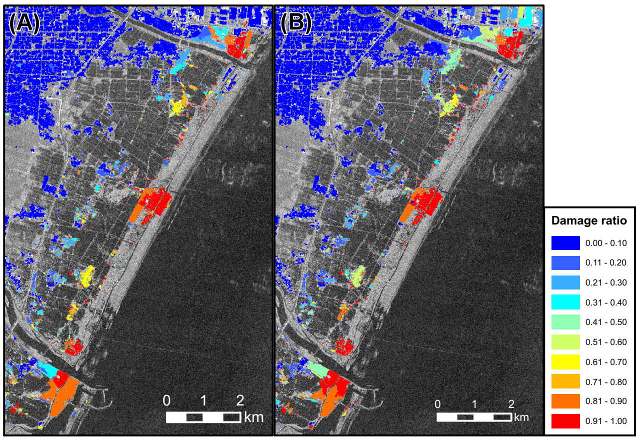

Fig. 8. Sendai damage estimation results. (A) Estimated results, (B) Truth data.

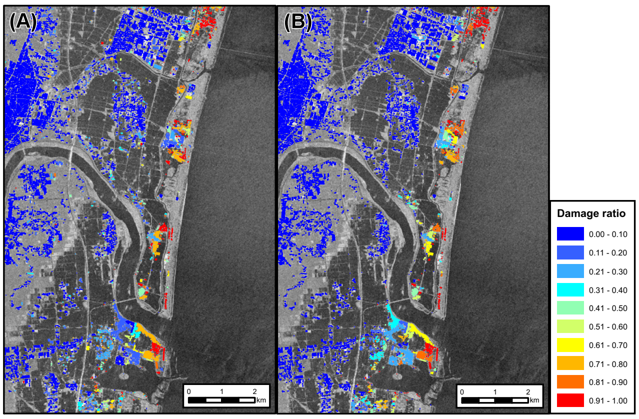

Fig. 9. Watari (town) damage estimation results. (A) Estimated results, (B) Truth data.

3.7. Damage Estimation

To estimate building damage, we multiplied damage function and correlation coefficient values in each object. Results for the damage estimation in Sendai were as shown in **Figs. 8(A)**, **(B)**. Comparing these figures confirms good agreement. When we estimated the number of damaged buildings in each object by multiplying the estimated damage ratio and the number of builidings, the number of damaged buildings in estimated results and ground truth data showed a high correlation, i.e., a Pearson's correlation coefficient of 0.99 (**Fig. 10(A)**).

To test transferability, we applied the function to Watari, located in southern Miyagi Prefecture as shown in (**Figs. 9(A)**, **(B)**). The correlation of the number of damaged buildings agreed well between estimated results and ground truth, resulting in a correlation coefficient of 0.98 as shown in (**Fig. 10(B)**).

4. Semiautomation on ArcGIS

Although the approach in the previous section showed high performance, the method cannot be applied without building footprint data being available. Our proposed

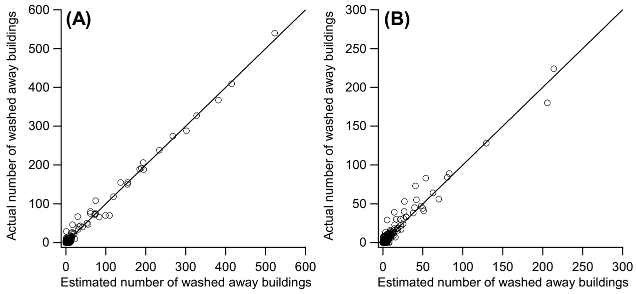

Fig. 10. Quantitative damage estimation evaluation. (A) Sendai (B) Watari.

method also is not automated, which it should be, considering emergency response situations. To address these problems, we address the development of an improved semiautomated model that does not require building footprint data.

4.1. Detecting Built-Up Areas

We detected built-up areas based on the method proposed by Esch et al. (2010) [21], i.e., detecting built-up areas from preevent TerraSAR-X data without using building footprint data. The model, as shown in **Fig. 11**, that the local deviation from the fully developed speckle, speckle divergence $D_{x,y}$, increases with the rising amount of actual structures within the resolution cell. The summarized accuracy of an object-based approach and a simplified pixel-based approach proposed by Esch et al. (2010) proved the object-based approach to provide slightly more accurate results than the pixel-based approach, but we wanted to develop a simplified tool that worked on ArcGIS. For this reason, we adopted the simplified pixel-based approach.

This approach consisted of the following two steps:

1 Texture analysis for pre-processing.

2 Classification of built-up areas by a pixel-based analysis.

4.1.1. Texture Analysis

To estimate multiplicative noise in SAR data, we derived coefficient of variation C by using the following equation:

$$C = \frac{\sigma}{\mu} \quad (3)$$

where μ is the mean value and σ is the standard deviation estimated with a pixel window. Theoretical C due to speckle is calculated by using the inverse of equivalent number of looks (ENL) as follows:

$$C = 1/ENL = 1/(L_a + L_r) \quad (4)$$

where L_a and L_r are the equivalent number of looks in the azimuth and range used to process raw data. In the case of TerraSAR-X data, L_a and L_r are provided by the meta-

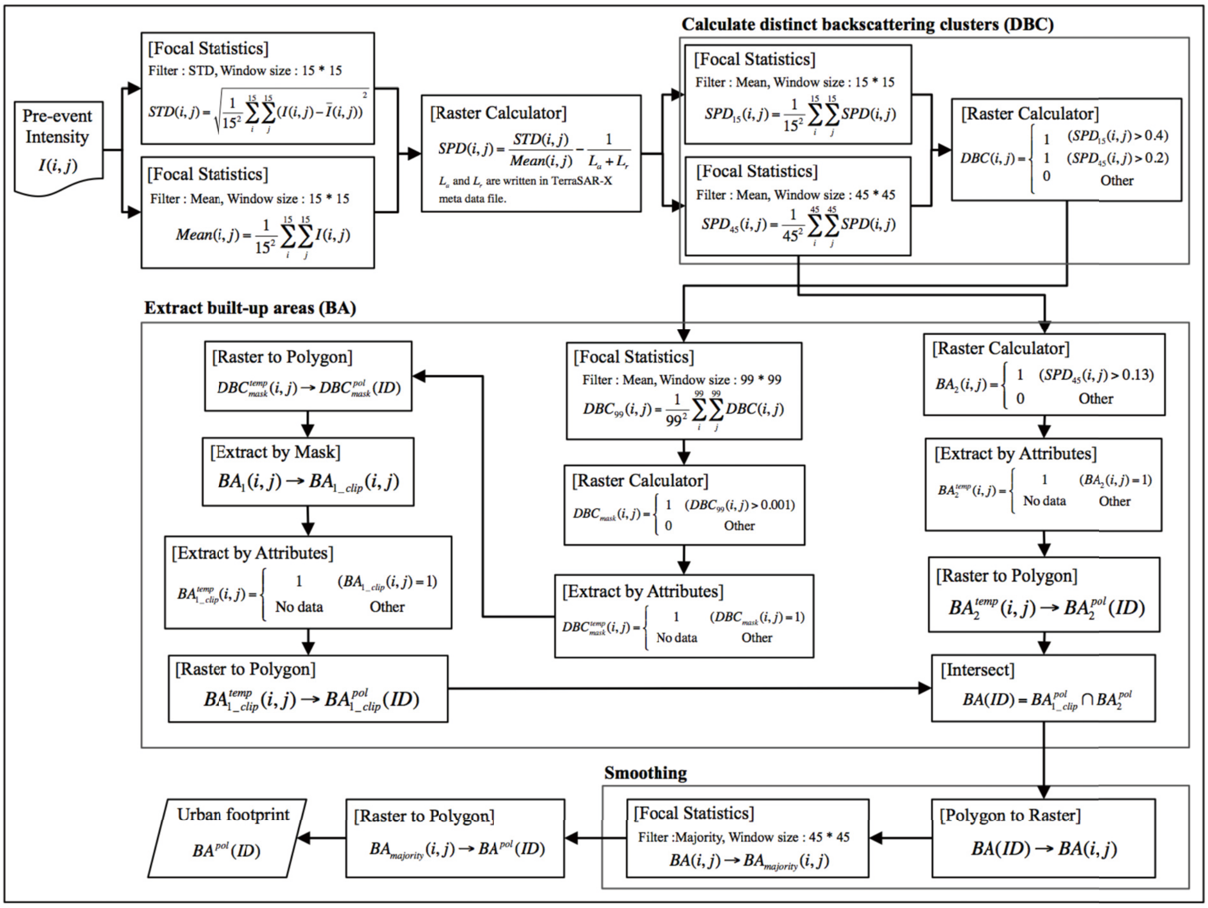

[] : Name of a tool equipped on ArcGIS, *BA* : built-up areas, *DBC* : distinct backscattering clusters, *I* : intensity values of TerraSAR-X data, *ID* : the given number for respective shape files, *i,j* : a location of a pixel, *SPD* : speckle divergence, *Mean* : mean values, *STD* : standard deviation

Fig. 11. Built-up area detection models in an ArcGIS environment. We revised parameters from the model of Esch et al. (2010).

data file. Next, local speckle divergence $D_{x,y}$ calculated by using the following equation:

$$D_{x,y} = C_{x,y} - C, \quad \text{with} \quad C_{x,y} = \frac{\sigma_{x,y}}{\mu_{x,y}} \quad . \quad . \quad . \quad . \quad . \quad (5)$$

where $\mu_{x,y}$ is the mean value and $\sigma_{x,y}$ is the standard deviation of TerraSAR-X intensity data estimated with a 11.25 m×11.25 m pixel window. The parameter C, the coefficient of variation, represents the theoretical heterogeneity due to the fully developed speckle.

4.1.2. Pixel-Based Image Analysis

Built-up areas were extracted based on speckle divergence. Parameters were referred to from Esch et al.(2010). The transferability of the parameter was verified in the paper. In the first step, we compared locally (18.75 m × 18.75 m) and regionally (56.25 m × 56.25 m) averaged $D_{x,y}$ to two thresholds, i.e., 0.4 and 0.2. If one of the thresholds was exceeded, areas were classified into distinct backscattering clusters (DBC). In the second step, built-up areas (BA) were detected if the region included a certain amount of DBC within a 123.75 m × 123.75 m pixel window, and a regionally increased $D_{x,y}$ exceeds 0.001, which is described as $DBC_{99} > 0.001$ in **Fig. 11**. Next, we integrated all DBC areas into class BA and assigned all other unclassified pixels assigned as nonbuilt-up areas (NBA). We then applied a 56.25 m × 56.25 m majority filter to eliminate outliers, obtaining the final built-up areas shown in **Fig. 12(A)**. Black represents building footprint data and the silhouette is detected built-up areas. In this result, the estimated silhouette of built-up areas is much larger than the actual building footprint.

The critical parameter for the size of detected built-up areas is threshold value $DBC_{99} > 0.001$ as shown in **Fig. 11**. This becomes smaller as the threshold value increases, but detected results of built-up areas were overestimated compared to the actual building footprint. To minimize the detected result, we testee several types of threshold value DBC_{99} from 0.1 to 0.5 as shown in **Figs. 12(B)** to **(F)**. The detected silhouette of built-up areas should be closer to the building footprint described in black in **Fig. 12**, but should not be smaller than actual building footprint data. **Figs. 12(B)** to **(E)** shows that the size of extracted built-up areas becomes smaller as the DBC value becomes higher. Comparing building footprint data to the detected silhouette, we selected threshold $DBC_{99} = 0.4$, which agrees well with building footprint data. If DBC_{99} is less than 0.4, the extracted silhouette of built-up areas becomes too large, increasing nonbuilding areas. This makes it difficult to estimate damage accurately. If DBC_{99} is higher than 0.4, however, the extracted silhouette becomes too small.

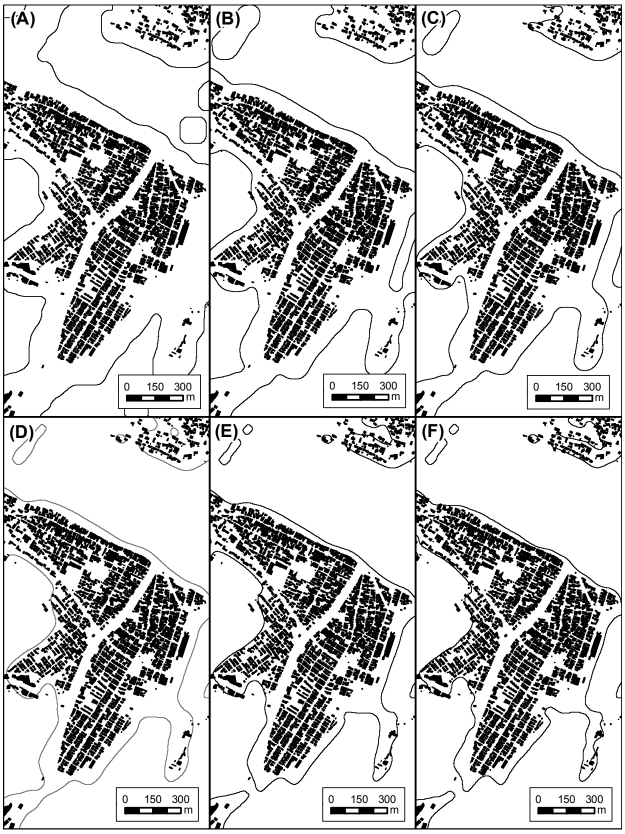

Fig. 12. Evaluation of parameters for detecting built-up areas. The threshold values were (A) $DBC_{99} > 0.001$, (B) $DBC_{99} > 0.1$, (C) $DBC_{99} > 0.2$, (D) $DBC_{99} > 0.3$, (E) $DBC_{99} > 0.4$ and (F) $DBC_{99} > 0.5$.

4.1.3. Implementation on ArcGIS

We implemented these procedures on ArcGIS with model builder platform. The model is shown in **Fig. 11**. We had to choose TerraSAR-X intensity data. We also had to input *ENL* values. As we ran the model, a shape file of built-up areas was exported.

4.2. Result and Discussion in Detecting Built-Up Areas

The result of detecting built-up areas is shown in **Fig. 13**. Compared to preevent building footprint data published by Zenrin in Japan, we confirmed that extracted built-up areas fully covered building footprint data. Some parts showed overestimations in detecting built-up areas, however, e.g., a highway running north to south showed higher speckle divergence and was extracted as built-up areas. Bridges and other parts were also classified as built-up areas because, speckle divergence showed higher values in areas where high and low backscattering existed too close to each other. In the case of the highway, layover and double bounce scattering enhanced backscattering coefficients at the foot of the highway. The road showed darker backscattering, which was caused by specular scattering. A man-made structure was detected successfully so in that sense, the model worked well. We focused on detecting residential area, so it was necessary to resolve such under- and overestimation when estimating building damage.

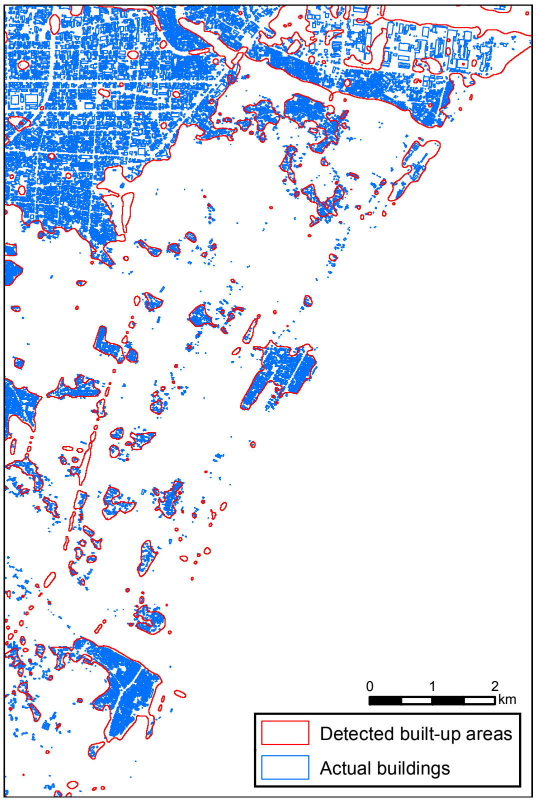

Fig. 13. Built-up area detection results.

It would also be of value to discuss the stability of speckle divergence values. Eq. (5) shows that speckle divergence calculates the local variablity of sigma nought values. We consider local variability in built-up areas to show stably high values because man-made structures cause an extremely high sigma nought due to layover or double-bounce scattering and extremely low sigma nought due to radar shadows.

4.3. Damage Estimation

Damage ratio was estimated based on the damage function and correlation coefficient. To apply the method for a quick response, the method was automated on ArcGIS environment. However, ArcGIS environment does not support the region growing algorithm. Therefore, the more simplified tile scale approach was adopted in this case.

Tile sizes of 100, 150, 200, . . ., 400 meters were examined. To determine the optimal tile size, Pearson's correlation coefficient of the actual building damage and estimated result was calculated as the index of damage ratio or the number of buildings in the tile. The results are summarized in the **Table 1**.

To estimate detailed building damage, the tile size should be smaller, but based on **Table 1**, we found that the correlation between actual damage and estimated results increased as tile size increased. One reason for this was that, when the tile was too small, the number of buildings included in the tile might also be too small and damage

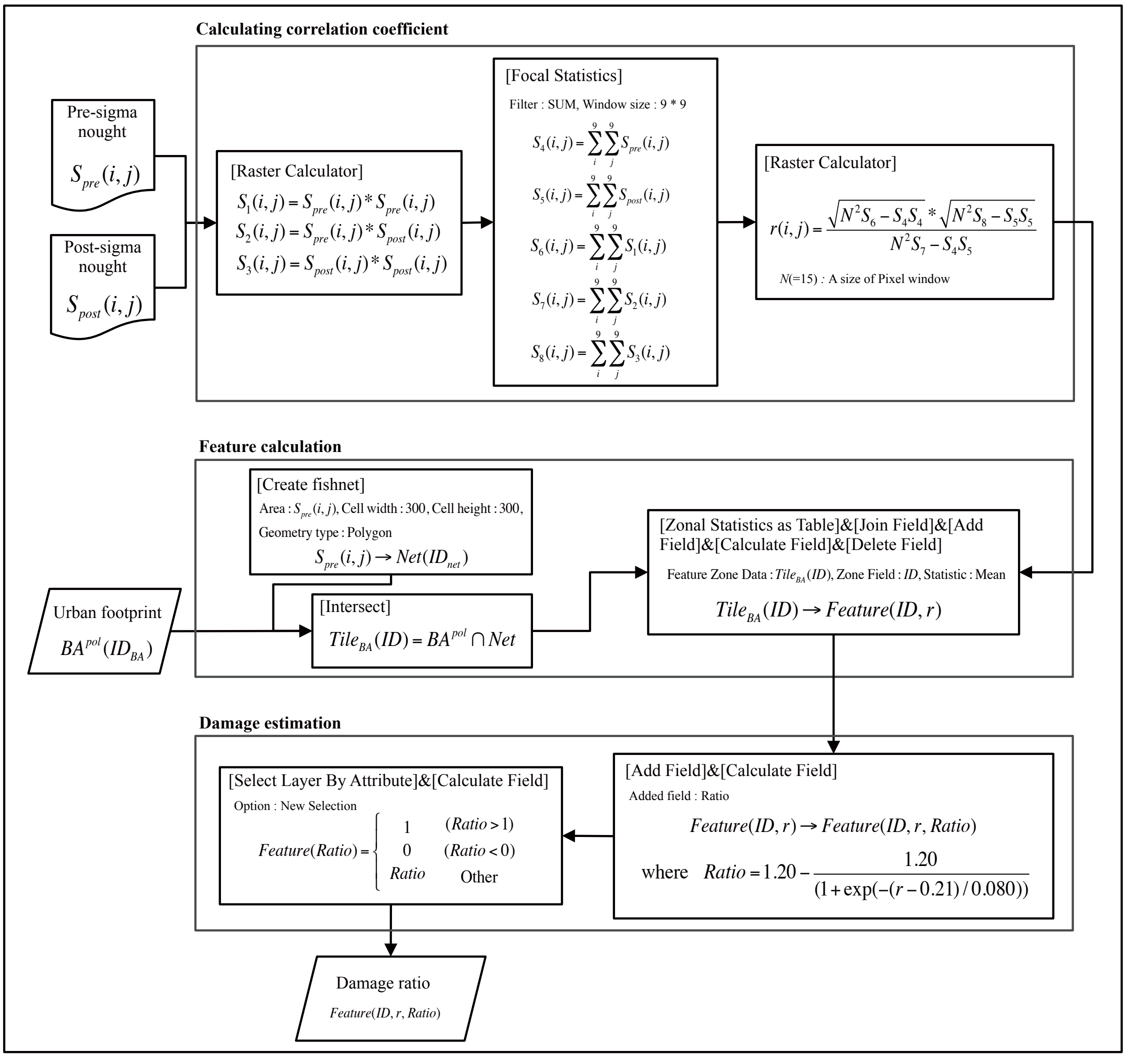

[] : name of a tool equipped on ArcGIS, *Active* : activated shape files by the selecting tools, *Area* : the area of the shape file, *BA* : a shape file of built-up areas, *D* : the values of elevation (m), *Feature* : estimated feature values at a tile scale, *i,j* : a location of a pixel, *N* : a size of pixel window, *Net* : a shape file of tiles, *r* : correlation coefficient, , *Ratio* : Damage ratio, *S* : temporal results of calculations based on the sigma nought values, S_{pre},S_{post} : pre- and post-event sigma nought values, *Tile* : a shape file of tiles inside built-up areas

Fig. 14. Building damage estimation model in the ArcGIS environment.

Table 1. Evaluation for tile size calculation.

Tile size	Num.	R01	Truth	Estimate	R02
100	1894	0.54	5347	5619	0.97
150	1029	0.58	5341	5653	0.98
200	689	0.64	5345	5670	0.99
250	523	0.58	5340	5685	0.99
300	379	0.65	5331	5716	0.99
350	308	0.66	5331	5695	0.99
400	267	0.70	5345	5762	0.99

Num.: Number of tiles in inundation zones. R01: Pearson's correlation coefficient of damage ratio between estimated result and ground truth. Truth: Total number of actual damaged buildings. Estimate: Total number of damaged buildings estimated by function. R02: Pearson's correlation coefficient of the number of damaged buildings between estimated results and ground truth

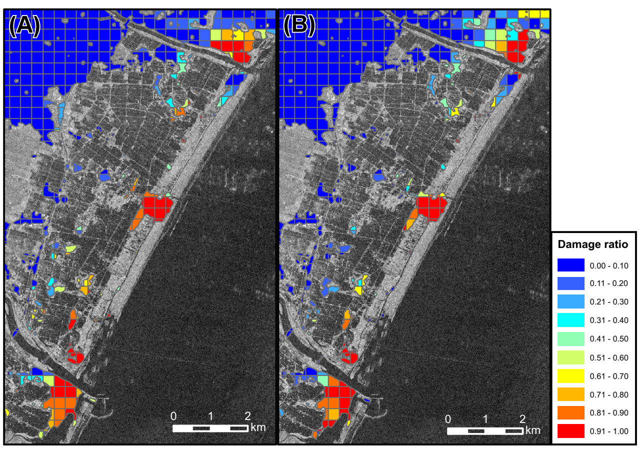

Fig. 15. Building damage estimation results using a semi-automated tool. (A) Estimated results, (B) Truth data.

might not be estimated well. Pearson's correlation coefficient of the number of damaged buildings in R02 showed a higher value than that of the damage ratio in R01 because damage estimation accuracy depends on the number of buildings included in each tile. If this number were too large, the relationship between the damage ratio and the correlation coefficient value might be stronger, but accuracy assessment based on the damage ratio in R01 ig-

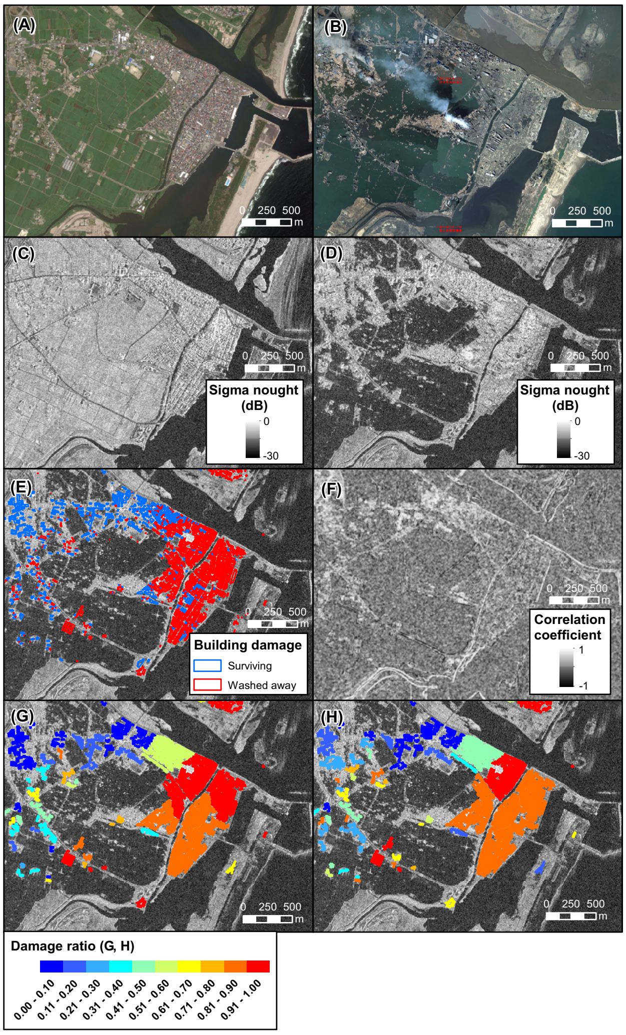

Fig. 16. Example of optical debris area images where the improved model worked well. (A) Preevent, (B) Postevent, (C) Preevent TerraSAR-X data, (D) Postevent TerraSAR-X data, (E) Building damage, (F) Correlation coefficient image, (G) Estimated damage ratio, (H) Actual damage ratio.

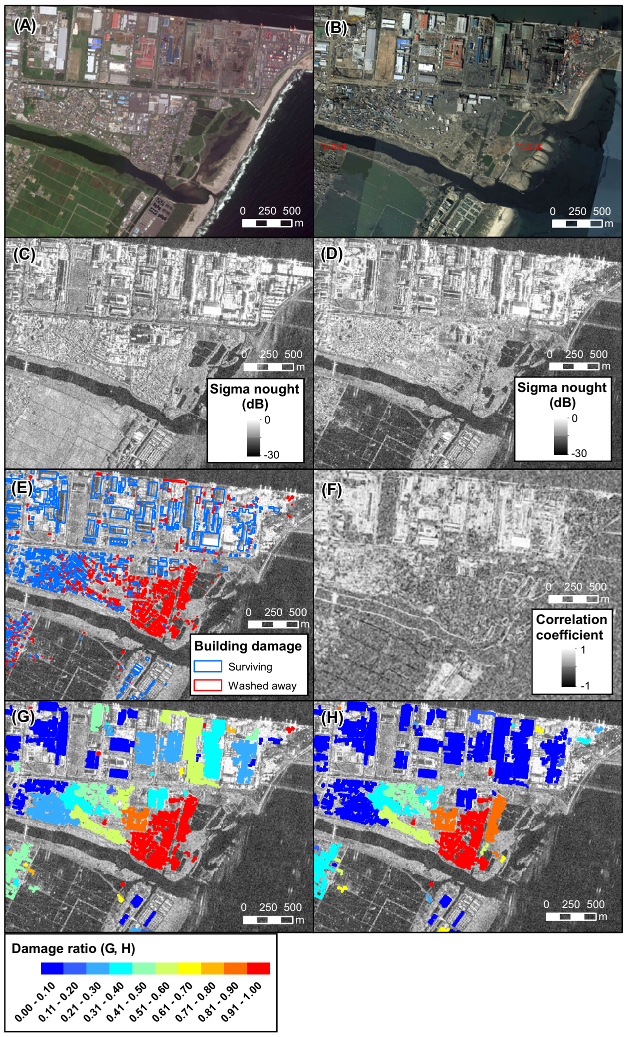

Fig. 17. Example of false optical image negative in large-scale building areas. (A) Preevent, (B) Postevent, (C) Preevent TerraSAR-X data, (D) Postevent TerraSAR-X data, (E) Building damage, (F) Correlation coefficient image, (G) Estimated damage ratio, (H) Actual damage ratio.

nores the number of buildings in each tile, so accuracy in R02 shows a higher value than the value in R01. Comparing results from several types of tile size, we found that overes timations in nondamaged areas disappeared as tile size reached 300 m, so we used a tile of 300 m. Note, however, that analysis that is more sensitive to tile size would be needed for applications in the future.

We ran the process on ArcGIS using the structure of the model in **Fig. 14**. Damage estimation results are shown in **Fig. 15**. It took 26 minutes to detect built-up areas and estimate building damage in Sendai using a semi-automated tool in the ArcGIS environment (Images:277 MB,CPU:3.7GHz).

5. Results and Discussion

Comparing results estimated for building damage and truth data, we confirmed good agreement between estimated results and actual damage data. Main improvement could be seen especially in debris-filled areas, where analysis is difficult based on a building-unit scale as shown in **Fig. 16**. Comparing the actual damage ratio and estimated results, we confirmed good agreement regarding washed-away buildings. Debris and buildings at left in **Fig. 16** show the areas where surviving buildings and debris are mixed, and where estimating damage on a building unit scale was difficult. We have improved this as described in this paper and have proven that the model work in complicated damaged areas.

Figures 17(A), (B) confirmed underestimations in parts in the northern part of the figure. To determine why, we compared results with pre- and postevent optical images, correlation coefficient images, and TerraSAR-X data (**Fig. 17**). We found that large-scale buildings were concentrated in these areas. We thus inferred that large-scale buildings not destroyed in a tsuami disaster resulted in mean correlation coefficient values for objects with higher values, even if the damage ratio was increased by damage.

We concluded that physical reasons inducing the high performance in other areas was explained by radar properties in built-up areas. Man-made structures showed high backscatter in layover areas and low backscatters in shadow areas. These radar properties are dominant and consistent with other built-up areas. In this study, we have focused on changes based on correlation coefficient values, and these are highly related to changes in layover and shadow areas. We could thus infer that applying this model to other test sites has a high possibility, as shown in the case of Watari. Even under different topographic conditions such as ria coasts, we believe that the model works well because layover and shadow area configurations are the same in different time series if buildings are not adversely affected by a tsunami.

The semiautomated model worked well on ArcGIS on the whole, which is valuable in emergency situations. The quality of results is worse, however, than in object-oriented analysis. This means that the tile-based method should be used for quick response for preliminary results and the object-oriented method should be applied otherwise.

6. Conclusions

The main findings in this study are as follows:

(1) We developed a damage function for estimating the damage ratio of washed-away buildings that needs correlation coefficient calculated from high-resolution SAR data.

(2) We improved our proposal's applicability to areas in which buildings and debris were mixed, and improved estimations of building damage.

(3) We estimated the amount of buildings damaged by multiplying estimated damage ratios and the number of buildings in each object, validating this using an actual building damage map showing a Pearson's correlation coefficient of 0.99 in Sendai and 0.98 in Watari.

(4) We semi-automated a simplified model of our proposed approach on ArcGIS.

Acknowledgements

This research was supported financially by Grants-in-Aid for Scientific Research project numbers 15H06107, 25242035, and 24241059; Grant-in-Aid for JSPS Fellows project number 245839), the Core Research for Evolutional Science and Technology (CREST) program "Establishing the most advanced disaster reduction management system by fusion of real-time disaster simulation and big data assimilation." The authors received TerraSAR-X data from the Pasco Co. as part of a collaborative project.

References:

[1] The 2011 Tohoku Earthquake Tsunami Joint Survey Group (TTJS), "Report from survey group," http://www.coastal.jp/tsunami2011/ [referred on October 2013]

[2] National Police Agency, "Report of the Damage Caused by the 2011 Tohoku Earthquake and Tsunami" (in Japanese), http://www.npa.go.jp/archive/keibi/biki/higaijokyo.pdf [referred on October 2013]

[3] S. Koshimura, S. Hayashi, and H. Gokon, "Lessons from the 2011 Tohoku Earthquake Tsunami Disaster," Journal of Disaster Research, Vol.8, No.4, pp. 549-560, 2013.

[4] S. Koshimura, S. Hayashi, and H. Gokon, "The Impact of the 2011 Tohoku Earthquake Tsunami Disaster and Implications to the Reconstruction," Soils and Foundations, 2014.

[5] F. Dell'Acqua and P. Gamba, "Remote Sensing and Earthquake Damage Assessment: Experiences, Limits, and Perspectives," Proceedings of the IEEE, Vol.100, No.10, October 2012.

[6] M. Matsuoka and F. Yamazaki, "Use of Satellite SAR Intensity Imagery for Detecting Building Areas Damaged due to Earthquakes," Earthquake Spectra Vol.20, No.3, pp. 975-994, 2004.

[7] M. Matsuoka and F. Yamazaki, "Building Damage Mapping of the 2003 Bam, Iran, Earthquake Using Envisat/ASAR Intensity Imagery," Earthquake Spectra Vol.21, No.S1, S285-S294, 2005.

[8] M. Matsuoka, S. Koshimura, and N. Nojima, "Estimation of Building Damage Ratio due to Earthquakes and Tsunamis Using Satellite SAR Imagery," Geoscience and Remote Sensing Symposium (IGARSS), 2010 IEEE International, pp. 3347-3349, July 2010.

[9] M. Matsuoka and M. Estrada, "Development of Earthquake-induced Building Damage Estimation Model Based on ALOS/PALSAR Observing the 2007 Peru Earthquake," Journal of Disaster Research, Vol.8, No.2, pp.346-355, 2013.

[10] D. Brunner, G. Lemoine, and L. Bruzzone, "Earthquake Damage Assessment of Buildings Using VHR Optical and SAR Imagery," IEEE Transactions on Geoscience and Remote Sensing, Vol.48, No.5, May 2010.

[11] W. Liu, F. Yamazaki, H. Gokon, and S. Koshimura, "Extraction of Tsunami-flooded Areas and Damaged Buildings in the 2011 Tohoku-oki Earthquake from TerraSAR-X Intensity Images," Earthquake Spectra, Vol.29, No.S1, pp. S183-S200, 2013.

[12] W. Liu, F. Yamazaki, H. Gokon, and S. Koshimura, "Extraction of Damaged Buildings due to the 2011 Tohoku," Japan Earthquake and Tsunami, Proceedings of Geoscience and Remote Sensing Symposium (IGARSS), pp. 4038-4041, 2012.

[13] S. Chen and M. Sato, "Tsunami Damage Investigation of Built-up Areas Using Multitemporal Spaceborne Full Polarimetric SAR Images," IEEE Transactions on Geoscience and Remote Sensing, Vol.51, No.4, April 2013.

[14] M. Sato, S. Chen, and M. Satake, "Polarimetric SAR Analysis of Tsunami Damage Following the March 11, 2011 East Japan Earthquake," Proceedings of the IEEE, Vol.100, No.10, October 2012.

[15] M. Watanabe, T. Motohka, Y. Miyagi, C. Yonezawa, and M. Shimada, "Analysis of Urban Areas Affected by the 2011 Off the Pacific Coast of Tohoku Earthquake and Tsunami with L-Band SAR Full-polarimetric Mode," IEEE Geoscience and Remote Sensing Letters, Vol.9, No.3, May 2012.

[16] F. Yamazaki, Y. Iwasaki, W. Liu, T. Nonaka, and T. Sasagawa, "Detection of Damage to Building Side-walls in the 2011 Tohoku," Japan Earthquake Using High-resolution TerraSAR-X Images, SPIE 8892, Image and Signal Processing for Remote Sensing XIX, 889212, 2013.

[17] Geospatial Information Authority of Japan (GSI), "Information of the 2011 Tohoku Earthquake and Tsunami," 2011, http://www.gsi.go.jp/BOUSAI/h23_tohoku.html [accessed April 1, 2011]

[18] Tohoku University, "Building Damage Map for the 2011 Tohoku Earthquake and Tsunami," 2011, http://www.tsunami.civil.tohoku.ac.jp/tohoku2011/mapping_damage.html [accessed July 1, 2015]

[19] A. Lopes, R. Touzi, and E. Nezry, "Adaptive Speckle Filters and Scene Heterogeneity," IEEE Transactions on Geoscience and Remote Sensing, Vol.28, No.6, pp. 992-1000, 1990.

[20] H. Gokon and S. Koshimura, "Mapping of Building Damage of the 2011 Tohoku Earthquake Tsunami in Miyagi Prefecture," Coastal Engineering Journal, Vol.54, No.1, 2012.

[21] T. Esch, T. Michael, S. Andreas, A. Roth, A. Müller, and S. Dech, "Delineation of Urban Footprints From TerraSAR-X Data by Analyzing Speckle Characteristics and Intensity Information," IEEE Transactions on Geosciene and Remote Sensing, Vol.48, No.2, February 2010.

Name:
Hideomi Gokon

Affiliation:
Assistant Professor, Institute of Industrial Science, the University of Tokyo

Address:
4-6-1-Be604, Komaba, Meguro-ku, Tokyo 153-8505, Japan

Brief Career:
2012-2015 Doctoral Course Student, Graduate School of Engineering, Tohoku University
2012-2015 JSPS Research Fellow (DC1)
2012 Visiting Researcher of German Aerospace Center (DLR)
2015-present Assistant Professor, Institute of Industrial Science, the University of Tokyo

Selected Publications:
- H. Gokon, J. Post, E. Stein, S. Martinis, A. Twele, M. Mück, C. Geiß, S. Koshimura, and M. Matsuoka, "A Method for Detecting Devastated Buildings by the 2011 Tohoku Earthquake Tsunami Using Multi-temporal TerraSAR-X Data," Geoscience and Remote Sensing letters, IEEE, 2015.
- H. Gokon, S. Koshimura, K. Imai, M. Matsuoka, Y. Namegaya, and Y. Nishimura, "Developing Fragility Functions for the Areas Affected by the 2009 Samoa Earthquake and Tsunami," Natural Hazards and Earth System Sciences, Vol.14, pp. 3231-3241, 2014.
- H. Gokon and S. Koshimura, "Mapping of Building Damage of the 2011 Tohoku Earthquake Tsunami in Miyagi Prefecture," Coastal Engineering Journal, Vol.54, No.1, 1250006, p. 12, 2012.

Academic Societies & Scientific Organizations:
- Japan Society of Civil Engineers (JSCE)

Name:
Shunichi Koshimura

Affiliation:
Professor, Dr. Eng., International Research Institute of Disaster Science (IRIDeS), Tohoku University

Address:
Aoba 468-1, Aramaki, Aoba, Sendai 980-0845, Japan

Brief Career:
2000- JSPS Research Fellows (PD)
2002- Research Scientist, Disaster Reduction and Human Renovation Institute
2005- Associate Professor, Graduate School of Engineering, Tohoku Univ.
2012- Professor, International Research Institute of Disaster Science (IRIDeS), Tohoku University

Selected Publications:
- E. Mas, B. Adriano, and S. Koshimura, "An Integrated Simulation of Tsunami Hazard and Human Evacuation in La Punta, Peru," Journal of Disaster Research, Vol.8, No.2, pp. 285-295, 2013.
- S. Koshimura, T. Oie, H. Yanagisawa, and F. Imamura, "Developing fragility functions for tsunami damage estimation using numerical model and post-tsunami data from Banda Aceh, Indonesia," Coastal Engineering Journal, JSCE, Vol.51, No.3, pp. 243-273, 2009.
- S. Koshimura, Y. Namegaya, and H. Yanagisawa, "Tsunami Fragility – A new measure to assess tsunami damage," Journal of Disaster Research, Vol.4, No.6, pp. 479-488, 2009.

Academic Societies & Scientific Organizations:
- Japan Society of Civil Engineers (JSCE)
- Institute of Social Safety Science (ISSS)
- Japan Association for Earthquake Engineering (JAEE)
- Japan Society for Computational Engineering and Science (JSCES)
- American Geophysical Union (AGU)

Name:
Masashi Matsuoka

Affiliation:
Associate Professor, Graduate School of Science and Technology, Tokyo Institute of Technology

Address:
4259-G3-2, Nagatsuta, Midori-ku, Yokohama 226-8502, Japan

Brief Career:
1992 Research Associate, Tokyo Institute of Technology
1996 Engineer, Remote Sensing Technology of Japan
1998 Deputy Team Leader, RIKEN
2004 Team Leader, National Research Institute for Earth Science and Disaster Prevention
2007 Senior Research Scientist, National Institute of Advanced Industrial Science Technology
2010 Division Chief, National Institute of Advanced Industrial Science Technology
2012- Associate Professor, Tokyo Institute of Technology

Selected Publications:
- Matsuoka and Yamazaki, "Use of Satellite SAR Intensity Imagery for Detecting Building Areas Damaged due to Earthquakes," Earthquake Spectra, EERI, Vol.20, No.3, pp. 975-994, 2004.
- Matsuoka and Nojima, "Building Damage Estimation by Integration of Seismic Intensity Information and Satellite L-band SAR Imagery," Remote Sensing, MDPI, Vol.2, No.9, pp. 2111-2126, 2010.
- Matsuoka and Yamazaki, "Comparative Analysis for Detecting Areas with Building Damage from Several Destructive Earthquakes Using Satellite Synthetic Aperture Radar Images," Journal of Applied Remote Sensing, SPIE, Vol.4, 041867, 2010.

Academic Societies & Scientific Organizations:
- Earthquake Engineering Research Institute (EERI)
- Architectural Institute of Japan (AIJ)
- Remote Sensing Society of Japan (RSSJ)